Experimental and Computational Investigation of Vinoxy and 1-Methylvinoxy Radicals from the Unimolecular Decay of Alkyl-Substituted Criegee Intermediates

Victoria P. Barber[a,*], Vincent J. Esposito[a], Tarek Trabelsi[b], Anne S. Hansen[a], Trent A. McHenry[a], Joseph S. Francisco[a,b], and Marsha I. Lester[a,†]

[a]Department of Chemistry, University of Pennsylvania, Philadelphia, PA 19104-6323
[b]Department of Earth and Environmental Sciences, University of Pennsylvania, Philadelphia, PA 19104-6316

VPB: https://orcid.org/0000-0003-4543-4657
VJE: https://orcid.org/0000-0001-6035-3869
TT: https://orcid.org/0000-0001-6258-7191
ASH: https://orcid.org/0000-0002-6285-586X
TAH: https://orcid.org/0000-0001-7690-7950
JSF: http://orcid.org/0000-0002-5461-1486
MIL: http://orcid.org/0000-0003-2367-3497

Abstract

Unimolecular decay of s*yn*-alkyl substituted Criegee intermediates, which form in the atmosphere via alkene ozonolysis, is an important source of vinoxy radicals, intermediates in many atmospheric processes. Vinoxy, CH_2CHO, and 1-methylvinoxy, CH_3CH_2CO, were previously generated from alternative photochemical pathways and investigated spectroscopically. Here, vinoxy and 1-methylvinoxy are generated from the *syn*-CH_3CHOO and $(CH_3)_2COO$ Criegee intermediates, and detected via UV laser-induced fluorescence (LIF) on the $\widetilde{B}\,^2A''$-$\widetilde{X}\,^2A''$ transition. Comparison with previously reported LIF spectra provides definitive identification of the vinoxy and 1-methylvinoxy radicals. High level, multireference calculations of the $\widetilde{B}$-$\widetilde{X}$ transition energies agree well with experiment.

* Present address: Civil and Environmental Engineering and Chemical Engineering Departments, MIT, Cambridge, MA 02139
† Corresponding author email: milester@sas.upenn.edu

1. Introduction

Vinoxy radicals (CH_2CHO) and substituted analogues with vinoxy functionality ($C(R_1R_2)C(R_3)O$) are intermediates in a number of atmospheric and combustion processes [1]. One important source of vinoxy radicals in the troposphere is alkene ozonolysis. In this reaction, ozone adds across a C=C double bond to form a primary ozonide (POZ), which then decomposes to yield a carbonyl oxide, known as the Criegee intermediate, as well as a carbonyl coproduct. The alkene ozonolysis reaction is highly exothermic, and the nascent Criegee intermediates are therefore formed with a high degree of internal excitation[2]. Some portion of the Criegee intermediates will promptly undergo unimolecular decomposition. The remaining Criegee intermediates will be collisionally stabilized, and either undergo thermal unimolecular decay [2] or bimolecular reactions with other atmospheric species [3].

For simple, substituted Criegee intermediates with an α alkyl H-atom in the *syn* position, the primary atmospheric removal pathway is predicted to be unimolecular reaction [4], which occurs via a 1,4 H-atom transfer mechanism and is shown in Scheme 1. The α H-atom transfers to the terminal oxygen of the carbonyl oxide group to yield a vinyl hydroperoxide (VHP) intermediate. The VHP then rapidly decomposes to yield OH, along with a radical with vinoxy functionality [5,6]. The initial substituents of the Criegee intermediate will determine the corresponding substituents of the vinoxy analogue, as shown in Scheme 1. While much experimental work exists on OH production from Criegee intermediates [4–6], neither vinoxy radicals nor their substituted analogues have been directly detected from the unimolecular decay of Criegee intermediates prior to this report.

In previous laboratory studies, vinoxy radicals and their methyl-substituted analogues, 1-methylvinoxy and 2-methylvinoxy, have been generated via 193 nm photolysis of vinyl-substituted ethers, or by the reaction of alkenes (ethene and propene) with $O(^3P)$ atoms [7–11]. Thus, there is extensive experimental work on their spectroscopy. Vinoxy, 1-methylvinoxy, and 2-methylvinoxy have been detected via laser induced fluorescence (LIF) on their $\widetilde{B}\ ^2A''$-$\widetilde{X}\ ^2A''$ electronic transition. The LIF

spectrum of the simplest vinoxy radical was first observed by Inoue and Akimoto in a fast-flow reactor cell [7]. Subsequent work further characterized the LIF spectrum as well as the dispersed fluorescence spectrum (DF) of the vinoxy radical under both jet-cooled [8,12] and ambient conditions [9]. The jet-cooled LIF and DF spectra are vibrationally resolved, and are assigned based on theoretical calculations of the vibrational modes in both the $\widetilde{B}\ ^2A''$ and $\widetilde{X}\ ^2A''$ electronic states. The vibrationally resolved features within the $\widetilde{B}$-$\widetilde{X}$ system also exhibit rotational structure, allowing for the determination of the geometric structure of the vinoxy radical. The LIF spectrum of 1-methylvinoxy has also been reported.[10,13] Again, the LIF spectrum is vibrationally resolved, and provides information about the vibrational modes of 1-methylvinoxy in the $\widetilde{B}\ ^2A''$ state.

Previous theoretical investigations have been performed on the electronic structure and energetics of vinoxy and substituted vinoxy species using different multireference methods.[14–17] The optically allowed $\widetilde{B}$-$\widetilde{X}$ transition, between states with A″ symmetry, has been studied using multiconfigurational self-consistent field (MCSCF) methods, followed by mutireference configuration interaction (MRCI), to characterize the electronic structure changes associated with this transition in vinoxy [15,17], 1-methylvinoxy [15], 2-methylvinoxy [14], and halogen-substituted [15] vinoxy systems. Additionally, Matsika and Yarkony studied the photodissociation of vinoxy upon $\widetilde{B}$-$\widetilde{X}$ excitation and suggested that vinoxy dissociates to hydrogen and ketene products by nonadiabatic pathways [17]. Table S1 summarizes the theoretical and experimental $\widetilde{X}$ state rotational constants and $\widetilde{B}$-$\widetilde{X}$ electronic transition energies reported in the literature.

In 2012, an alternative synthetic method was developed to efficiently produce Criegee intermediates via photolysis of a diiodoalkyl species and subsequent reaction with oxygen [18]. In this laboratory, this method has been coupled to a free jet expansion to generate cold, stabilized Criegee intermediates in a collision free environment, including *syn*-CH_3CHOO [6], $(CH_3)_2COO$ [5], and most recently $(CH_3)(CH_3CH_2)COO$ [19]. UV LIF on the OH $\widetilde{A}$-$\widetilde{X}$(1,0) transition has been employed to detect OH radicals from the unimolecular decay of these Criegee intermediates [5,6,19]. Initially, OH products

from the unimolecular decay of internally excited *syn*-CH_3CHOO were detected at early times following 248 nm photolysis of CH_3CHI_2 in the presence of O_2 [20]. Infrared (IR) excitation was used to provide cold Criegee intermediates with the energy required to surmount or tunnel through the TS barrier (15-18 kcal mol^{-1} depending on the Criegee intermediate [5,6,19]) for the 1,4 H-atom transfer reaction that leads to OH radical products, which were again detected by UV LIF.

In this work, we present the first direct detection of vinoxy radicals and a substituted analogue produced from the unimolecular decay of Criegee intermediates. Two alkyl substituted Criegee intermediates are investigated, *syn*-CH_3CHOO and $(CH_3)_2COO$, which decay *via* the 1,4 H-atom transfer mechanism to produce OH and vinoxy or 1-methylvinoxy products, respectively [5,6]. Vibrationally-resolved LIF spectra of the $\widetilde{B}$-$\widetilde{X}$ electronic transition are recorded for each species, allowing for unambiguous identification of the vinoxy radicals. The experimental results are paired with *ab initio* calculations utilizing high-level multireference methods in order to characterize the electronic structure and $\widetilde{B}$-$\widetilde{X}$ electronic transition energy of each species.

2. Methods

2.1 Experimental Method

The generation of the *syn*-CH_3CHOO and $(CH_3)_2COO$ Criegee intermediates in a pulsed supersonic expansion has been described previously [5,6]. Briefly, the 1,1-diiodoethane (CH_3CHI_2) or 2,2-diiodopropane ($(CH_3)_2CI_2$) is entrained in a 20% O_2/Ar gas mixture at a backing pressure of 25 psig and pulsed through a pulsed valve (Parker Hannefin Series 9), which is gently heated to ca. 50 °C using a Peltier Thermoelectric module in order to increase the vapor pressure of the diiodoalkane precursor. The gas pulse travels through a quartz capillary reactor tube (1 mm ID, 25 mm length), and into vacuum. The diiodo alkane precursor is photolyzed with 355 nm radiation from a frequency tripled Nd:YAG laser (Continuum Powerlite 8000, ca. 20 mJ/pulse, 6 ns FWHM, 10 Hz), which is cylindrically focused onto the tip of the capillary. The resulting monoiodo radical (CH_3CHI or $(CH_3)_2CI$) reacts with O_2 to produce the Criegee intermediate (*syn*-CH_3CHOO or $(CH_3)_2COO$, respectively).

In previous experiments, 248 nm light from a KrF excimer laser (Coherent COMPEX 50) was used to photolyze the diiodoalkane precursors. These precursors also absorb 355 nm light, albeit slightly less strongly [21,22]. The 355 nm excitation also results in C-I bond dissociation (ca. 50 kcal mol^{-1}) [23], and provides ca. 30 kcal mol^{-1} of excess energy. The resultant monoiodo radical then reacts with O_2 to form the Criegee intermediate.

While the detailed energetics associated with the formation of *syn*-CH_3CHOO and $(CH_3)_2COO$ from their respective diiodoalkane precursors have not been reported, these processes are expected to be analogous to the formation of the simplest Criegee intermediate formaldehyde oxide (CH_2OO) from its diiodoprecursor, CH_2I_2 [23,24]. Velocity map imaging (VMI) studies of the photodissociation of CH_2I_2 estimate that 80% of the excess energy from photolysis is partitioned into the resulting CH_2I monoiodo radical [23,24]. When the CH_2I radical reacts with O_2 (a nearly thermoneutral process with an enthalpy of reaction of ca. 1 kcal mol^{-1}) [25], it is anticipated that a large portion of the energy will be retained as internal excitation of the nascent CH_2OO Criegee intermediate.

Given a similar process for the formation of *syn*-CH_3CHOO and $(CH_3)_2COO$, it is expected that at least 80% of the excess energy from 355 nm photolysis of CH_3CHI_2 or $(CH_3)_2CI_2$ is partitioned into internal excitation of the resulting alkyl-substituted CH_3CHI or $(CH_3)_2CI$ radicals. The actual energy partitioning to internal excitation of the monoiodo radicals may be greater due to the larger number of vibrational degrees of freedom of the substituted monoiodo radicals compared to CH_2I. Assuming a similar, nearly thermoneutral O_2 addition to the CH_3CHI or $(CH_3)_2CI$ radicals, some portion of the resulting *syn*-CH_3CHOO and $(CH_3)_2COO$ Criegee intermediates are born with high enough internal energy to undergo prompt unimolecular decay prior to collisional cooling. The OH and vinoxy or 1-methylvinoxy radicals that result from the prompt decay of *syn*-CH_3CHOO or $(CH_3)_2COO$, respectively, are cooled in the supersonic expansion alongside the remaining Criegee intermediates and other components of the gas mixture.

Approximately 1 cm downstream from the tip of the capillary, in the collision-free region of the expansion, the gas mixture is intersected by a UV laser beam, which excites the cold vinoxy radicals on

their $\widetilde{B}\ ^2A''$-$\widetilde{X}\ ^2A''$ transition. Tunable UV radiation (0.5-3 mJ/pulse depending on wavelength, 5 ns FWHM, 0.08 cm^{-1} resolution) is generated by frequency doubling (InRad Autotracker III, KDP-C Crystal) the output of an Nd:YAG (Continuum Powerlite 7020, 10 Hz) pumped dye laser (Continuum ND6000, LDS 698 dye), which is loosely focused to a diameter of ca. 2 mm in the interaction region. The frequency doubled dye laser output is scanned across a portion of the $\widetilde{B}\ ^2A''$-$\widetilde{X}\ ^2A''$ spectrum for each of the vinoxy radicals; the frequency of the dye laser is calibrated using a wavemeter (Coherent WaveMaster). Low resolution survey scans are performed at a high scan speed (2 points/cm^{-1}). The resulting fluorescence is detected with a gated photomultiplier tube (Electron Tubes 9813QB) after passing through a 400 nm bandpass filter (Thorlabs FBH400-40, center wavelength: 400 nm, bandwidth: 40 nm, maximum transmission: >90%), which spans the central portion of the vinoxy DF spectrum.[8] The signal is preamplified and captured on a digital storage oscilloscope (LeCroy Waverunner 44Xi) which is interfaced with a computer for processing. Based on previously reported fluorescence lifetimes [8,10], the fluorescence signal was integrated for 220 ns following the UV probe laser pulse.

2.2 Computational Method

Electronic structure calculations of the ground ($\widetilde{X}$) and second excited ($\widetilde{B}$) electronic states of vinoxy and 1-methylvinoxy were performed using Complete Active Space Self-Consistent Field (CASSCF) followed by single-point energy calculations using multireference configuration interaction (MRCI) including the Davidson correction (MRCI+Q) [26–29]. In the calculations, all atoms were described using the aug-cc-pVTZ basis set [30]. For the CASSCF wave function, the active space consisted of freezing the 6 and 10 lowest doubly occupied molecular orbitals in vinoxy and 1-methylvinoxy, respectively, with the remaining valence orbitals treated as active. In the MRCI calculations, the same active space was used and all configurations in the CI expansion of the CASSCF wave function having a weight larger than 0.04 were considered. For a more accurate characterization of the equilibrium geometry, rotational constants, and harmonic vibrational frequencies of the ground state, we also used the standard coupled-cluster theory with single and double excitations, including a

perturbative treatment of triple (CCSD(T)) [31,32]. All calculations were performed using MOLPRO 2019.1 [33].

3. Results and Discussion

We present LIF spectra attributed to the vinoxy and 1-methylvinoxy radical. In the first case, the LIF spectrum is acquired following photolysis of the CH_3CHI_2 precursor, where the resulting monoiiodo radical reacts with O_2 to yield the *syn*-CH_3CHOO Criegee intermediate. The *syn*-CH_3CHOO undergoes unimolecular decay to OH and the vinoxy radical; the resultant LIF spectrum obtained in the 28750-30000 cm^{-1} range is shown in Figure 1. In the second case, the LIF spectrum is acquired following photolysis of the $(CH_3)_2CI_2$ precursor, where the resulting monoiodo radical reacts with O_2 to yield the $(CH_3)_2COO$ Criegee intermediate. Here, the $(CH_3)_2COO$ undergoes unimolecular decay to produce OH and the 1-methylvinoxy radical. The resultant LIF spectrum acquired in the 27700-28020 cm^{-1} range is shown in Figure 2.

Based on comparison to previously published spectra [8,10,13], we identify the spectra shown in Figures 1 and 2 as arising from the $\widetilde{B}$-$\widetilde{X}$ transitions of the vinoxy and 1-methylvinoxy radicals, respectively. This assignment is consistent with the predicted mechanisms for the unimolecular decay of the *syn*-CH_3CHOO and $(CH_3)_2COO$, which produce either the vinoxy or the 1-methylvinoxy radical, respectively, as the coproducts of OH. In each case, only a portion of the spectrum is scanned; the spectra have been extensively mapped previously [8,10,13], and a full analysis of the LIF spectrum is not the goal of this work. Instead, a small section of the spectrum is recorded in order to confirm the identity of the vinoxy or 1-methylvinoxy product. Table 1 provides a detailed comparison between key spectroscopic features observed in this work and those reported previously.

The LIF spectrum (Figure 1) taken following photolysis of the CH_3CHI_2 precursor is in excellent agreement with the LIF spectrum for the $\widetilde{B}\ ^2A''$-$\widetilde{X}\ ^2A''$ transition of vinoxy previously reported by Brock et al.[8] . We observe the electronic origin (0_0^0) at 28787 cm^{-1}, in good agreement with the previously reported value of 28784 cm^{-1} [8].

Adiabatic excitation energies were also calculated for the $\widetilde{B}$-$\widetilde{X}$ electronic transition of vinoxy. The MRCI+Q calculated value of 28445 cm^{-1} (Table 1) quantitatively agrees with the experimentally determined transition energy. At the CASSCF level, there is poor agreement with experiment, with the excitation energy predicted to be 30099 cm^{-1} (Table S2). This difference may be due to the exclusion of electron correlation. The MRCI level shows better agreement with experiment, and is calculated to be 29300 cm^{-1} (Table S2). However, for quantitative agreement between experiment and theory, the Davidson correction (MRCI+Q) is required, further improving the contribution of electron correlation to the energy.

From analysis of the calculated molecular orbitals (Figure 3), the $\widetilde{X}$ state singly occupied molecular orbital (SOMO) containing the unpaired electron has electron density concentrated along the vinyl C=C double bond; the radical site is located on the terminal carbon. The $\widetilde{B}$-$\widetilde{X}$ electronic transition consists of two main electron promotions. The larger contribution involves promotion of an electron from the highest occupied molecular orbital (HOMO-1) to the SOMO, which increases the bonding character of the C=C vinyl bond. A smaller contribution to this transition comes from the promotion of an electron from the SOMO to the lowest unoccupied molecular orbital (LUMO), shifting electron density from the C=C vinyl bonding interaction to an anti-bonding orbital across the carbonyl double bond.

Two other high-intensity experimentally observed features, which are shifted to higher frequency relative to the electronic origin by 920 cm^{-1} and 1121 cm^{-1}, are also in good agreement with previously reported features [8,12]. These features have been previously assigned to the 8_0^1 and 7_0^1, where ν_8 (920 cm^{-1}) is the CC stretching mode and ν_7 (1121 cm^{-1}) is the CH_2 scissor mode [8,12]. Small differences in relative intensities of features are seen in the present study compared to prior work [8], which are likely due to experimental factors (e.g. filters). As shown in Figure S1 several weak features are observed at lower energy than the electronic origin. Based on comparison with the previously reported LIF spectrum of vibrationally hot vinoxy [34], these are ascribed to vibrational hot bands of the vinoxy radical, indicating incomplete vibrational cooling of the vinoxy radical in the supersonic expansion.

$\widetilde{B}$ state harmonic vibrational frequencies calculated at the CASSCF level are reported in Table S3 and agree well with previously reported theoretical values [35]. The calculated value for ν_7 of 1150 cm^{-1} is 29 cm^{-1} larger than the experimentally observed feature (no anharmonic corrections). The calculated value for ν_8 of 926 cm^{-1} also agrees well with the experimentally observed feature assigned to ν_8, differing by only 6 cm^{-1}.

An expanded view of the 0_0^0 transition is shown in Figure 4. The observed rotational band contour is well-represented by a simulation in PGOPHER using experimentally determined ground and excited state rotational constants for the vinoxy radical [8,11,36], a low rotational temperature of 15 K, and an a/b type transition, in agreement with previously reported results [8]. Computed rotational constants for the $\widetilde{X}$ and $\widetilde{B}$ electronic states of vinoxy, reported in Table 2, are in excellent agreement with available experimental data [8,11], providing further confirmation that the spectral carrier is indeed the vinoxy radical, which is rotationally cooled in the jet expansion. In addition, the observed fluorescence lifetime (see Figure S2) is in accord with that reported by Brock et al. of 190 ± 2 ns [8].

The LIF spectrum (Figure 2) taken following photolysis of the $(CH_3)_2CI_2$ precursor has several intense features that can be clearly attributed to the $\widetilde{B}\ ^2A'' - \widetilde{X}\ ^2A''$ transition of 1-methylvinoxy, based on comparison to the previously reported LIF spectrum by Williams et al. [10,13]. In this case, the electronic origin (0_0^0) has been previously reported at 27283 cm^{-1}, but has low intensity and was not scanned here [10,13].

Adiabatic excitation energies were calculated for the $\widetilde{B}$-$\widetilde{X}$ electronic transition of 1-methylvinoxy. The MRCI+Q calculated value of 27812 cm^{-1} for the adiabatic excitation energy agrees well with the previously observed electronic origin, and improves upon previously reported calculations.[15] The CASSCF calculated value of 28593 cm^{-1} showed poor agreement with experiment while the MRCI calculated value of 30212 cm^{-1} shows worse agreement (Table S2). For 1-methylvinoxy, the adiabatic excitation energy calculations differed greatly when restricting to C_1 or C_s symmetry, with C_1 symmetry yielding more accurate results across all levels of theory (Table S2). The inadequacy of the calculations

with C_s symmetry may stem from constrained orbital rotations necessary in C_s symmetry, the number of configurations, or the limited active space (see discussion in SI regarding symmetry).

The $\widetilde{B}$-$\widetilde{X}$ transition of 1-methylvinoxy is dominated by the promotion of an electron from the HOMO-1 to the SOMO, representing the promotion of electron density from the carbonyl double bond to the C=C vinyl bond. Again, a second, smaller, contribution comes from the promotion of an electron from the SOMO to the LUMO, moving electron density from the vinyl C=C bond to an anti-bonding orbital associated with the carbonyl double bond (see Figure 3).

We observe two strong features shifted to higher frequency relative to the electronic origin by 483 and 589 cm^{-1}, in accord with previously observed features (see Table 1) [10,13]. The observed feature at 589 cm^{-1} also exhibits a shoulder at 597 cm^{-1}, again in good agreement with previous results [10,13]. A pair of weaker features at relative frequencies of 681 and 714 cm^{-1} are also observed, in good agreement with a similarly shaped pair of previously reported features [10,13]. In the 1-methylvinoxy case, the assignment of the vibrationally resolved features in experimentally observed LIF spectrum is less straightforward than for vinoxy, due to the presence of a methyl torsional mode in both the ground and electronically excited state [10,13]. All five of the features discussed above are attributed to transitions between pure torsional levels in the ground and excited electronic states [13]. Additionally, we observe features between 28000-28200 cm^{-1} (see Figure S3) that have not been reported for jet-cooled 1-methylvinoxy and likely arise from another source, e.g. products from a reaction of 1-methylvinoxy with O_2, and will be explored in future work.

4. Atmospheric implications

In the atmosphere, the vinoxy radical and its substituted analogues may undergo unimolecular decay or bimolecular reaction. There are two potential pathways for unimolecular decay of the vinoxy radical[37]. The first is dissociation to yield ketene and an H atom. The second proceeds via rearrangement to an acetyl radical, followed by decomposition to yield a methyl radical and carbon monoxide. The first pathway is expected to dominate with a branching ratio of approximately 2:1[37].

The rates for these unimolecular reactions have not been reported, but the high barriers associated with them (ca. 40 kcal mol^{-1}) suggest they should be slow [38]. Detailed unimolecular reaction energetics for substituted vinoxy analogues have not been reported, but are assumed to proceed via similarly high barriers.

Bimolecular reaction of vinoxy radicals and their substituted analogues can occur with a variety of atmospheric species, most importantly O_2 [39–42]. The reaction with O_2 is predicted to be the most likely oxidation pathway of the vinoxy radical, due to the large atmospheric abundance of O_2 compared to other possible oxidants [26]. The reaction of vinoxy with O_2 has been shown experimentally to be quite fast, with rate constants on the order of 10^{-13} cm^3 s^{-1} at 298 K in the high pressure limit [39,41,42]. Rate constants 5-7 times faster than these have been observed for the reactions of 1-methylvinoxy ($CH_2C(CH_3)O$) and 2-methylvinoxy (CH_3CHCHO) with O_2 [40,43]. A summary of the rate constants for the reactions of various vinoxy-like radicals with O_2 is given in Table S4.

The fast reaction of vinoxy and 1-methylvinoxy with O_2 may explain why vinoxy radicals have not been observed in previous experiments on Criegee intermediates under thermal conditions (i.e. in flow tubes). Because Criegee intermediate synthesis in these experiments relies on the reaction of the monoiodo radical with O_2, there must be excess oxygen available in the system, which can quickly react with the vinoxy radicals. To some extent, it is surprising that these radicals are observed at all in this work, given that they are formed in the presence of excess oxygen in the capillary reactor tube. However, the vinoxy radicals are generated near the tip of the capillary reactor tube. This results in a brief residence time within the capillary reactor tube, which is apparently short compared to the reaction timescale. Subsequent supersonic expansion results in cooling (15 K rotational temperature) and isolation. These conditions enable the vinoxy radicals to survive and be detected by LIF in the interaction region.

The vinoxy + O_2 reaction proceeds by a nearly barrierless addition to the carbon-centered vinoxy radical to form an oxoalkylperoxy radical [38] (though the vinoxy radical in its ground state can be drawn in two resonance forms, with the radical site on either the oxygen or carbon atom, it is understood that the unpaired electron is primarily localized on the carbon atom) [44]. Substituted vinoxy analogues are

expected to react with O_2 via a similar mechanism [40,45]. These oxoalkylperoxy radicals are a subset of peroxy radicals (RO_2), which are important intermediates in a variety of atmospheric processes [46]. The newly formed oxoalkylperoxy radical may dissociate back to reactants, react with other atmospheric species, or undergo unimolecular decay or rearrangement.

Bimolecular reactions available to oxoalkylperoxy radicals in the atmosphere include reaction with HO_2 to yield peroxides, or with NO to yield alkoxy radicals or alkyl nitrates.[46] Unimolecular decay may occur via several different mechanisms to form various products (including OH radicals) [38,42,45]. Even more importantly though, the oxoalkylperoxy radicals associated with O_2 addition to larger vinoxy radicals may undergo autoxidation, whereby successive H-atom transfer reactions and O_2 additions yield low-volatility organic compounds that are implicated in the formation of secondary organic aerosols [47]. Recent experimental [47–49] and theoretical [50] work has shown that this autoxidation chemistry is of great importance in the ozonolysis of biogenic alkenes such as α-pinene, producing highly oxidized, multifunctional low volatility molecules that lead to particle growth. As unimolecular decay of Criegee intermediates, particularly large, biogenically-derived Criegee intermediates, is predicted to be to be a dominant atmospheric removal pathway[3], the production of vinoxy radicals represents an important radical propagation reaction in the atmosphere and a key connection between alkene ozonolysis and SOA formation.

5. Conclusion

Unimolecular decay of *syn*-CH_3CHOO and $(CH_3)_2COO$ has been shown to generate vinoxy and 1-methylvinoxy radicals, respectively, along with OH radicals. The vinoxy radicals are cooled in a supersonic expansion and detected by UV LIF on their $\widetilde{B}^2A''$-$\widetilde{X}^2A''$ transitions. The UV LIF spectra of vinoxy and 1-methylvinoxy have been reported previously, but the radicals were generated by different photochemical pathways [7–10,13]. Comparison between the LIF spectra presented herein and those reported previously provides unambiguous identification of each vinoxy radicals species. High-level *ab initio* calculations of the electronic structure of vinoxy and 1-methylvinoxy show that MRCI+Q adiabatic

excitation energies agree well with experiment. The strategy used here demonstrates that calculations performed in C_1 symmetry better characterize vinoxy radical species, and this technique can be extended to explore vinoxy species arising from larger and more complex Criegee intermediates. The reaction between vinoxy radicals and O_2 is a critical link between Criegee intermediates and RO_2 chemistry, and can lead to secondary organic aerosol formation in the atmosphere.

Acknowledgements

The experimental research was supported through the National Science Foundation under grant CHE-1664572 (MIL). This material is also based upon work supported by the National Science Foundation Graduate Research Fellowship Program under Grant No. DGE-1845298 (VJE). One of the authors (ASH) gratefully acknowledges support from the Carlsberg Foundation (CF18-0614) and the Independent Research Fund Denmark (9036-00016B). Any opinions, findings, and conclusions or recommendations expressed in this material are those of the author(s) and do not necessarily reflect the views of the National Science Foundation.

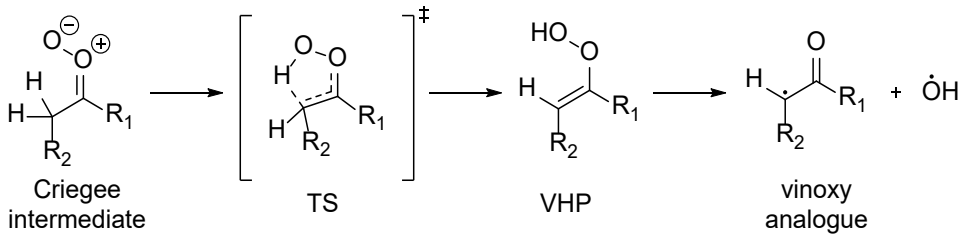

Scheme 1: Generic H-atom transfer reaction for Criegee intermediates to OH and vinoxy products. In this work, *syn*-CH_3CHOO (R_1=H, R_2=H) leads to vinoxy, while $(CH_3)_2COO$ (R_1=CH_3, R_2=H) yields 1-methyl vinoxy.

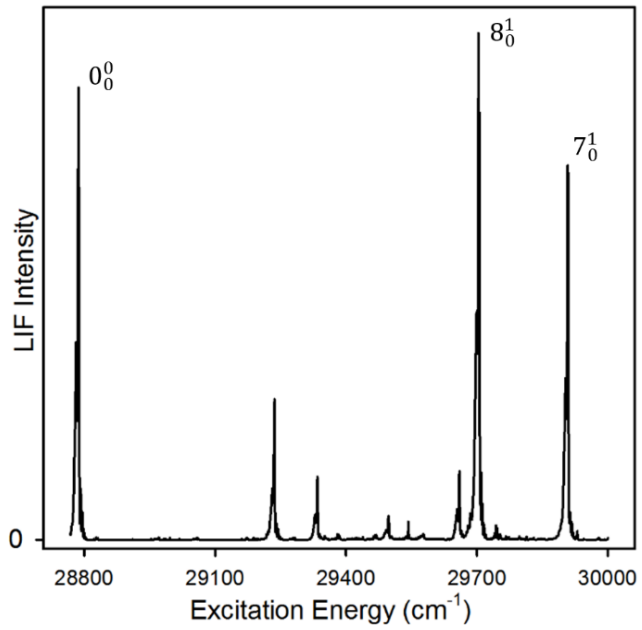

Figure 1: LIF spectrum taken following photolysis of CH_3CHI_2 and subsequent reaction of the resulting monoiodo radical with O_2 to form the *syn*-CH_3CHOO Criegee intermediate. The spectrum is attributed to the $\widetilde{B}$-$\widetilde{X}$ transition of the vinoxy radical, CH_2CHO, which forms from the unimolecular decay of the *syn*-CH_3CHOO and is cooled in the supersonic expansion, based on comparison with the previously reported spectrum for the vinoxy radical in Ref. [8]. Only the strongest features are labeled for simplicity.

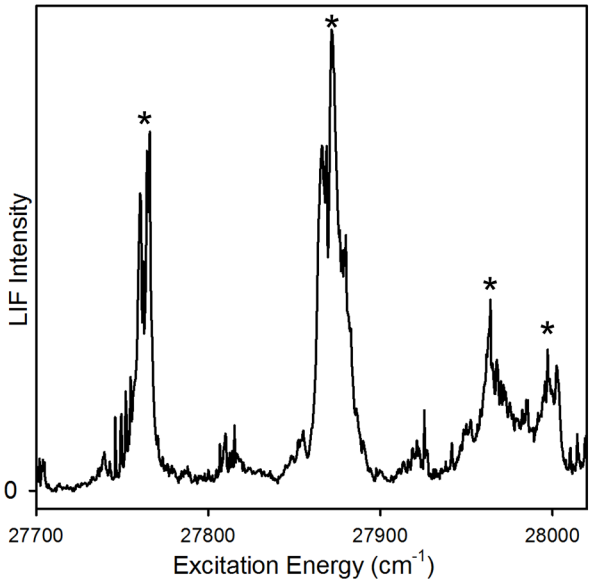

Figure 2: LIF spectrum taken following photolysis of $(CH_3)_2CHI_2$ and subsequent reaction of the resulting monoiodo radical with O_2 to form the $(CH_3)_2CHOO$ Criegee intermediate. The features with asterisks are discussed in the text, and attributed to the $\tilde{B}$-$\tilde{X}$ transition of the 1-methylvinoxy radical, $CH_2C(CH_3)O$, which forms from the unimolecular decay of the $(CH_3)_2CHOO$ and is cooled in the supersonic expansion. The assignment is based on comparison with the previously reported LIF spectra for the 1-methylvinoxy radical in Refs. [10] and [13]. Smaller features have also been observed previously in the LIF spectrum of the 1-methylvinoxy radical.

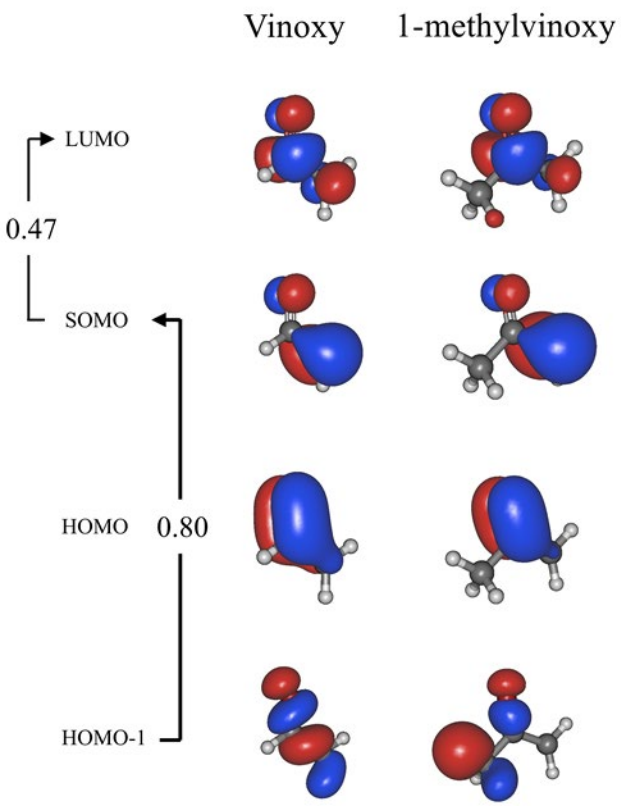

Figure 3: Frontier molecular orbitals of the $\widetilde{X}\,^2A''$ state for vinoxy and 1-methylvinoxy (isovalue=0.05) at the CASSCF/aug-cc-pVTZ level of theory. The arrows illustrate the orbital promotions (with weighting) that dominate the $\widetilde{B}$-$\widetilde{X}$ electronic transitions.

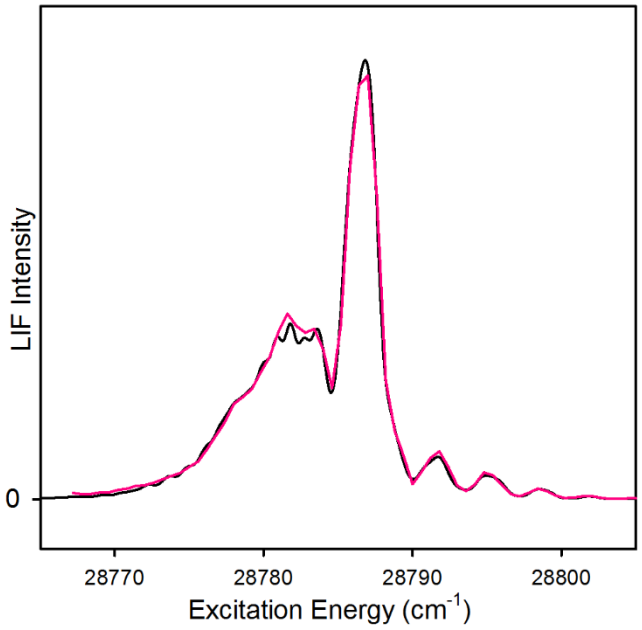

Figure 4: Expanded view of the 0_0^0 band observed in the experimental LIF spectrum of the $\widetilde{B}$-$\widetilde{X}$ transition of the vinoxy radical (red). The spectrum is overlayed with a rotational band contour (black) generated in PGOPHER [36], which uses previously determined rotational constants for the $\widetilde{X}$ [11] and $\widetilde{B}$ [8] states, an a/b-type (0.6/0.4) transition, and a rotational temperature of 15 K.

Table 1: Key peak positions from this work compared with prior reports, and comparison of experimental and theoretical band origins for the $\widetilde{B}$-$\widetilde{X}$ transition of vinoxy and 1-methylvinoxy.

Transition	Frequency (cm^{-1})				
	Absolute Position		Relative Position		
	Literature[a]	This Work[a]	Literature	This Work	Theory
			Vinoxy[b]		
0_0^0	28784	28787	0	0	28445[d] 28716[e]
8_0^1	29701	29707	917	920	
7_0^1	29906	29908	1122	1121	
			1-methylvinoxy[b]		
a	27283	-[c]	0	-[c]	27812[d] 28242[f]
d	27764	27766	481	483	
e	27869	27872	586	589	
e'	27881	27880	598	597	
f	27963	27964	680	681	
g	28002	27997	719	714	

[a] Transition frequencies are taken from peak positions, while those from literature are band origins.
[b] Band origins and labels for vinoxy and 1-methyl vinoxy from references [8] and [10,13], respectively.
[c] The electronic origin of 1-methylvinoxy has low signal and is not scanned in this work. Relative positions of observed peaks are based on the literature value for the band origin.
[d] This work (MRCI+Q/aug-cc-pVTZ).
[e] Ref. [17].
[f] Ref. [15].

Table 2: Rotational constants (in MHz) of vinoxy in the ground ($\widetilde{X}$) and second excited ($\widetilde{B}$) electronic states calculated using different levels of theory with the aug-cc-pVTZ basis set.

	Ground state ($\widetilde{X}\,^2A''$)			Second excited state ($\widetilde{B}\,^2A''$)	
	CCSD(T)	CASSCF	Experiment[a]	CASSCF	Experiment[b]
A	67092	67006	66676	63182	63232
B	11155	11471	11447	9995	10295
C	9564	9794	9758	8630	8961

[a] Ref. [11].
[b] Ref. [8].

References

[1] L. Vereecken, J.S. Francisco, Theoretical studies of atmospheric reaction mechanisms in the troposphere, Chem. Soc. Rev. 41 (2012) 6259–6293. https://doi.org/10.1039/c2cs35070j.

[2] G.T. Drozd, T. Kurtén, N.M. Donahue, M.I. Lester, Unimolecular Decay of the Dimethyl-Substituted Criegee Intermediate in Alkene Ozonolysis: Decay Time Scales and the Importance of Tunneling, J. Phys. Chem. A. 121 (2017) 6036–6045. https://doi.org/10.1021/acs.jpca.7b05495.

[3] M.A.H. Khan, C.J. Percival, R.L. Caravan, C.A. Taatjes, D.E. Shallcross, Criegee intermediates and their impacts on the troposphere, Environ. Sci. Process. Impacts. 20 (2018) 437–453. https://doi.org/10.1039/C7EM00585G.

[4] M.I. Lester, S.J. Klippenstein, Unimolecular Decay of Criegee Intermediates to OH Radical Products: Prompt and Thermal Decay Processes, Acc. Chem. Res. 51 (2018) 978–985. https://doi.org/10.1021/acs.accounts.8b00077.

[5] F. Liu, J.M. Beames, M.I. Lester, Direct Production of OH Radicals upon CH Overtone Activation of $(CH_3)_2COO$ Criegee Intermediates, J Chem Phys. 141 (2014) 234312. https://doi.org/10.1063/1.4903961.

[6] F. Liu, J.M. Beames, A.S. Petit, A.B. McCoy, M.I. Lester, Infrared-driven Unimolecular Reaction of CH_3CHOO Criegee Intermediates to OH Radical Products, Science. 345 (2014) 1596–1598.

[7] G. Inoue, H. Akimoto, Laser-induced fluorescence of the C_2H_3O radical, J. Chem. Phys. 74 (1981) 425–433. https://doi.org/10.1063/1.440848.

[8] L.R. Brock, E.A. Rohlfing, Spectroscopic studies of the $\tilde{B}\ ^2A''$-$\tilde{X}\ ^2A''$ system of the jet-cooled vinoxy radical, J. Chem. Phys. 106 (1997) 10048–10065. https://doi.org/10.1063/1.474091.

[9] K.I. Barnhard, M. He, B.R. Weiner, Excited-State Dynamics of CH2CHO ($\tilde{B}^2A$‘‘), J. Phys. Chem. 100 (1996) 2784–2790. https://doi.org/10.1021/jp952457e.

[10] S. Williams, E. Zingher, J.C. Weisshaar, $\tilde{B} \leftarrow \tilde{X}$ Vibronic Spectra and $\tilde{B}$-State Fluorescence Lifetimes of Methylvinoxy Isomers, J. Phys. Chem. A. 102 (1998) 2297–2301. https://doi.org/10.1021/jp980451u.

[11] Y. Endo, S. Saito, E. Hirota, The microwave spectrum of the vinoxy radical, J. Chem. Phys. 83 (1985) 2026–2034. https://doi.org/10.1063/1.449345.

[12] L.F. DiMauro, M. Heaven, T.A. Miller, Laser induced fluorescence study of the $\tilde{B}\ ^2A'' \rightarrow \tilde{X}\ ^2A''$ transition of the vinoxy radical in a supersonic free jet expansion, J. Chem. Phys. 81 (1984) 2339–2346. https://doi.org/10.1063/1.447932.

[13] S. Williams, L.B. Harding, J.F. Stanton, J.C. Weisshaar, Barrier to Methyl Internal Rotation of 1-Methylvinoxy Radical in the $\tilde{X}\ ^2A$" and $\tilde{B}\ ^2A$" States: Experiment and Theory, J. Phys. Chem. A. 104 (2000) 10131–10138. https://doi.org/10.1021/jp001009q.

[14] L.S. Alconcel, H.-J. Deyerl, R.E. Continetti, Effects of Alkyl Substitution on the Energetics of Enolate Anions and Radicals, J. Am. Chem. Soc. 123 (2001) 12675–12681. https://doi.org/10.1021/ja0120431.

[15] M. Yamaguchi, S. Inomata, N. Washida, Multireference Configuration Interaction Calculation of the $\tilde{B}\ ^2A''$–$\tilde{X}\ ^2A''$ Transition of Halogen- and Methyl-Substituted Vinoxy Radicals, J. Phys. Chem. A. 110 (2006) 12419–12426. https://doi.org/10.1021/jp0647840.

[16] D.I.G. Bennett, L.J. Butler, H.-J. Werner, Comparing electronic structure predictions for the ground state dissociation of vinoxy radicals, J. Chem. Phys. 127 (2007) 094309. https://doi.org/10.1063/1.2753489.

[17] S. Matsika, D.R. Yarkony, Photodissociation of the vinoxy radical through conical, and avoided, intersections, J. Chem. Phys. 117 (2002) 7198–7206. https://doi.org/10.1063/1.1507587.

[18] O. Welz, J.D. Savee, D.L. Osborn, S.S. Vasu, C.J. Percival, D.E. Shallcross, C.A. Taatjes, Direct Kinetic Measurements of Criegee Intermediate (CH_2OO) Formed by Reaction of CH_2I with O_2, Science. 335 (2012) 204–207. https://doi.org/10.1126/science.1213229.

[19] V.P. Barber, A.S. Hansen, Y. Georgievskii, S.J. Klippenstein, M.I. Lester, Experimental and theoretical studies of the doubly-substituted methyl-ethyl Criegee intermediate: Infrared action

spectroscopy and unimolecular decay to OH radical products, J. Chem. Phys. 152 (2020) In Press. https://doi.org/10.1063/5.0002422.
[20] L. Lu, J.M. Beames, M.I. Lester, Early time detection of OH radical products from energized Criegee intermediates CH_2OO and CH_3CHOO, Chem. Phys. Lett. 598 (2014) 23–27. https://doi.org/10.1016/j.cplett.2014.02.049.
[21] G. Schmitt, F.J. Comes, Photolysis of CH_2I_2 and 1,1-$C_2H_4I_2$ at 300 nm, J. Photochem. 14 (1980) 107–123. https://doi.org/10.1016/0047-2670(80)80002-5.
[22] Y.-P. Chang, C.-H. Chang, K. Takahashi, J.J.-M. Lin, Absolute UV Absorption Cross Sections of Dimethyl Substituted Criegee Intermediate $(CH_3)_2COO$, Chem. Phys. Lett. 653 (2016) 155–160. https://doi.org/10.1016/j.cplett.2016.04.082.
[23] B.W. Toulson, J.P. Alaniz, J. Grant Hill, C. Murray, Near-UV photodissociation dynamics of CH_2I_2, Phys. Chem. Chem. Phys. 18 (2016) 11091–11103. https://doi.org/10.1039/C6CP01063F.
[24] J.H. Lehman, H. Li, M.I. Lester, Ion Imaging Studies of the Photodissociation Dynamics of CH_2I_2 at 248 nm, Chem. Phys. Lett. 590 (2013) 16–21. https://doi.org/10.1016/j.cplett.2013.10.029.
[25] E.P.F. Lee, D.K.W. Mok, D.E. Shallcross, C.J. Percival, D.L. Osborn, C.A. Taatjes, J.M. Dyke, Spectroscopy of the Simplest Criegee Intermediate CH_2OO: Simulation of the First Bands in Its Electronic and Photoelectron Spectra, Chem. – Eur. J. 18 (2012) 12411–12423. https://doi.org/10.1002/chem.201200848.
[26] P.J. Knowles, H.-J. Werner, An Efficient Second Order MCSCF Method for Long Configuration Expansions, Chem. Phys. Lett. 115 (1985) 259–267. https://doi.org/10.1016/0009-2614(85)80025-7.
[27] H. Werner, P.J. Knowles, A second order multiconfiguration SCF procedure with optimum convergence, J. Chem. Phys. 82 (1985) 5053–5063. https://doi.org/10.1063/1.448627.
[28] H.-J. Werner, P.J. Knowles, An Efficient Internally Contracted Multiconfiguration Reference CI Method, J. Chem. Phys. 89 (1988) 5803–5814. https://doi.org/10.1063/1.455556.
[29] P.G. Szalay, R.J. Bartlett, Multi-reference averaged quadratic coupled-cluster method: a size-extensive modification of multi-reference CI, Chem. Phys. Lett. 214 (1993) 481–488. https://doi.org/10.1016/0009-2614(93)85670-J.
[30] T.H. Dunning, Gaussian basis sets for use in correlated molecular calculations. I. The atoms boron through neon and hydrogen, J. Chem. Phys. 90 (1989) 1007–1023. https://doi.org/10.1063/1.456153.
[31] P.J. Knowles, C. Hampel, H.-J. Werner, Coupled Cluster Theory for High Spin Open Shell Reference Wavefunctions, J. Chem. Phys. 99 (1993) 5219–5227. https://doi.org/10.1063/1.465990.
[32] P.J. Knowles, C. Hampel, H.-J. Werner, Erratum: “Coupled cluster theory for high spin, open shell reference wave functions” [J. Chem. Phys. **99** , 5219 (1993)], J. Chem. Phys. 112 (2000) 3106–3107. https://doi.org/10.1063/1.480886.
[33] H.-J. Werner, P.J. Knowles, G. Knizia, F.R. Manby, M. Schütz, P. Celani, W. Györffy, D. Kats, T. Korona, R. Lindh, A. Mitrushenkov, G. Rauhut, K.R. Shamasundar, T.B. Adler, R.D. Amos, S.J. Bennie, A. Bernhardsson, A. Berning, D.L. Cooper, M.J.O. Deegan, A.J. Dobbyn, F. Eckert, E. Goll, C. Hampel, A. Hesselmann, G. Hetzer, T. Hrenar, G. Jansen, C. Köppl, S.J.R. Lee, Y. Liu, A.W. Lloyd, Q. Ma, R.A. Mata, A.J. May, S.J. McNicholas, W. Meyer, T.F.M. III, M.E. Mura, A. Nicklass, D.P. O’Neill, P. Palmieri, D. Peng, K. Pflüger, R. Pitzer, M. Reiher, T. Shiozaki, H. Stoll, A.J. Stone, R. Tarroni, T. Thorsteinsson, M. Wang, M. Welborn, MOLPRO, version 2019.1, a package of ab initio programs, molpro, 2019.
[34] H. Su, R. Bersohn, Vibrational state distribution and relaxation of vinoxy radicals, J. Chem. Phys. 115 (2001) 217–224. https://doi.org/10.1063/1.1369602.
[35] D.L. Osborn, H. Choi, D.H. Mordaunt, R.T. Bise, D.M. Neumark, C.M.M. Rohlfing, Fast beam photodissociation spectroscopy and dynamics of the vinoxy radical, J. Chem. Phys. 106 (1997) 3049–3066. https://doi.org/10.1063/1.473419.
[36] C.M. Western, PGOPHER: A Program for Simulating Rotational, Vibrational and Electronic Spectra, J. Quant. Spectrosc. Radiat. Transf. 186 (2017) 221–242. https://doi.org/10.1016/j.jqsrt.2016.04.010.

[37] C.-S. Lam, J.D. Adams, L.J. Butler, The Onset of H + Ketene Products from Vinoxy Radicals Prepared by Photodissociation of Chloroacetaldehyde at 157 nm, J. Phys. Chem. A. 120 (2016) 2521–2536. https://doi.org/10.1021/acs.jpca.6b01256.
[38] J.D. Weidman, R.T. Allen, K.B. Moore, H.F. Schaefer, High-level theoretical characterization of the vinoxy radical (•CH_2CHO) + O_2 reaction, J. Chem. Phys. 148 (2018) 184308–184308. https://doi.org/10.1063/1.5026295.
[39] L. Zhu, G. Johnston, Kinetics and Products of the Reaction of the Vinoxy Radical with O_2, J. Phys. Chem. 99 (1995) 15114–15119. https://doi.org/10.1021/j100041a030.
[40] T. Oguchi, A. Miyoshi, M. Koshi, H. Matsui, N. Washida, Kinetic Study on Reactions of 1-and 2-Methylvinoxy Radicals with O_2, J. Phys. Chem. A. 105 (2001) 378–382. https://doi.org/10.1021/jp001826q.
[41] E. Delbos, C. Fittschen, H. Hippler, N. Krasteva, M. Olzmann, B. Viskolcz, Rate coefficients and equilibrium constant for the $CH_2CHO + O_2$ reaction system, J. Phys. Chem. A. 110 (2006) 3238–3245. https://doi.org/10.1021/jp054697s.
[42] K. Lorenz, D. Rhasa, R. Zellner, B. Fritz, Laser Photolysis - LIF Kinetic Studies of the Reactions of CH_3O and CH_2CHO with O_2 between 300 and 500 K, Berichte Bunsenges. Für Phys. Chem. 89 (1985) 341–342. https://doi.org/10.1002/bbpc.19850890346.
[43] M. Hassouna, E. Delbos, P. Devolder, B. Viskolcz, C. Fittschen, Rate and equilibrium constant of the reaction of 1-methylvinoxy radicals with O_2: $CH_3COCH_2 + O_2 \leftrightarrow CH_3COCH_2O_2$, J. Phys. Chem. A. 110 (2006) 6667–6672. https://doi.org/10.1021/jp0558270.
[44] M. Dupuis, J.J. Wendoloski, W.A. Lester, Electronic structure of vinoxy radical CH_2CHO, J. Chem. Phys. 76 (1982) 488–492. https://doi.org/10.1063/1.442749.
[45] K.T. Kuwata, A.S. Hasson, R.V. Dickinson, E.B. Petersen, L.C. Valin, Quantum Chemical and Master Equation Simulations of the Oxidation and Isomerization of Vinoxy Radicals, J. Phys. Chem. A. 109 (2005) 2514–2524. https://doi.org/10.1021/JP047299I.
[46] J.H. Kroll, J.H. Seinfeld, Chemistry of secondary organic aerosol: Formation and evolution of low-volatility organics in the atmosphere, Atmos. Environ. 42 (2008) 3593–3624. https://doi.org/10.1016/j.atmosenv.2008.01.003.
[47] F. Bianchi, T. Kurtén, M. Riva, C. Mohr, M.P. Rissanen, P. Roldin, T. Berndt, J.D. Crounse, P.O. Wennberg, T.F. Mentel, J. Wildt, H. Junninen, T. Jokinen, M. Kulmala, D.R. Worsnop, J.A. Thornton, N. Donahue, H.G. Kjaergaard, M. Ehn, Highly Oxygenated Organic Molecules (HOM) from Gas-Phase Autoxidation Involving Peroxy Radicals: A Key Contributor to Atmospheric Aerosol, Chem. Rev. (2019) 3472–3509. https://doi.org/10.1021/acs.chemrev.8b00395.
[48] T.F. Mentel, M. Springer, M. Ehn, E. Kleist, I. Pullinen, T. Kurtén, M. Rissanen, A. Wahner, J. Wildt, Formation of Highly Oxidized Multifunctional Compounds: Autoxidation of Peroxy Radicals formed in the Ozonolysis of Alkenes – Deduced from Structure–Product Relationships, Atmospheric Chem. Phys. 15 (2015) 6745–6765. https://doi.org/10.5194/acp-15-6745-2015.
[49] M. Ehn, E. Kleist, H. Junninen, T. Petäjä, G. Lönn, S. Schobesberger, M.D. Maso, A. Trimborn, M. Kulmala, D.R. Worsnop, A. Wahner, J. Wildt, T.F. Mentel, Gas phase formation of extremely oxidized pinene reaction products in chamber and ambient air, Atmospheric Chem. Phys. 12 (2012) 5113–5127. https://doi.org/10.5194/acp-12-5113-2012.
[50] T. Kurtén, M.P. Rissanen, K. Mackeprang, J.A. Thornton, N. Hyttinen, S. Jørgensen, M. Ehn, H.G. Kjaergaard, Computational Study of Hydrogen Shifts and Ring-Opening Mechanisms in α-Pinene Ozonolysis Products, J. Phys. Chem. A. 119 (2015) 11366–11375. https://doi.org/10.1021/acs.jpca.5b08948.